Journal of Physics B: Atomic, Molecular and Optical Physics

ACCEPTED MANUSCRIPT

Binding of two-electron metastable states in semiconductor quantum dots under a magnetic field

To cite this article before publication: Mariano Garagiola *et al* 2018 *J. Phys. B: At. Mol. Opt. Phys.* in press https://doi.org/10.1088/1361-6455/aab1a0

Manuscript version: Accepted Manuscript

Accepted Manuscript is "the version of the article accepted for publication including all changes made as a result of the peer review process, and which may also include the addition to the article by IOP Publishing of a header, an article ID, a cover sheet and/or an 'Accepted Manuscript' watermark, but excluding any other editing, typesetting or other changes made by IOP Publishing and/or its licensors"

This Accepted Manuscript is **© 2018 IOP Publishing Ltd**.

During the embargo period (the 12 month period from the publication of the Version of Record of this article), the Accepted Manuscript is fully protected by copyright and cannot be reused or reposted elsewhere.
As the Version of Record of this article is going to be / has been published on a subscription basis, this Accepted Manuscript is available for reuse under a CC BY-NC-ND 3.0 licence after the 12 month embargo period.

After the embargo period, everyone is permitted to use copy and redistribute this article for non-commercial purposes only, provided that they adhere to all the terms of the licence https://creativecommons.org/licences/by-nc-nd/3.0

Although reasonable endeavours have been taken to obtain all necessary permissions from third parties to include their copyrighted content within this article, their full citation and copyright line may not be present in this Accepted Manuscript version. Before using any content from this article, please refer to the Version of Record on IOPscience once published for full citation and copyright details, as permissions will likely be required. All third party content is fully copyright protected, unless specifically stated otherwise in the figure caption in the Version of Record.

View the article online for updates and enhancements.

This content was downloaded from IP address 200.16.16.13 on 22/02/2018 at 18:56

Binding of two-electron metastable states in semiconductor quantum dots under a magnetic field

Mariano Garagiola

Facultad de Matemática, Astronomía, Física y Computación, Universidad Nacional de Córdoba and IFEG-CONICET, Ciudad Universitaria, X5000HUA Córdoba, Argentina

E-mail: mgaragiola@famaf.unc.edu.ar

Federico M. Pont

Facultad de Matemática, Astronomía, Física y Computación, Universidad Nacional de Córdoba and IFEG-CONICET, Ciudad Universitaria, X5000HUA Córdoba, Argentina

E-mail: pont@famaf.unc.edu.ar

Omar Osenda

Facultad de Matemática, Astronomía, Física y Computación, Universidad Nacional de Córdoba and IFEG-CONICET, Ciudad Universitaria, X5000HUA Córdoba, Argentina

E-mail: osenda@famaf.unc.edu.ar

Abstract. Applying a strong enough magnetic field results in the binding of few electrons resonant states. The mechanism was proposed many years ago but its verification in laboratory conditions is far more recent. In this work we study the binding of two-electron resonant states. The electrons are confined in a cylindrical quantum dot which is embedded in a semiconductor wire. The geometry considered is similar to the one used in actual experimental setups. The low energy two-electron spectrum is calculated numerically from an effective mass approximation Hamiltonian modelling the system. Methods for binding thresholds calculations in systems with one- and two-electrons are thoroughly studied, in particular, we use quantum information quantities to asses when the strong lateral confinement approximation can be used to obtain reliable low-energy spectra. For reasons of simplicity, only cases without bound states in the absence of external field are consider. Under this conditions, the binding threshold for the one-electron case is given by the lowest Landau energy level. Moreover, the energy of the one-electron bounded resonance can be used to obtain the two-electron binding threshold. It is shown that for realistic values of the two-electron model parameters it is feasible to bind resonances with field strengths of few tens of Teslas.

Accepted Manuscript

1. Introduction

The manifold role that semiconductor nano-structures play in today Physics include, among others, to be a test bed to check basic tenets of Quantum Mechanics. The Aharonov-Bohm effect has been verified measuring oscillatory persistent currents in different settings [1], but the ability to charge semiconductor nano-structures with few electrons put the experiment in semiconductor rings close to the requirements of the gedanken experiment situation [2], moreover this effect can be observed using electrons, holes or neutral excitons [3]. Indeed, the fact that there is no limitation in the number of electrons charging a given nano-structure, together with interferometric techniques, are the main elements that enable the control of solid-state flying qubits [4]. Also, the interference between two indistinguishable electrons is possible in these setups [5]. Additionally it has been proposed an experiment to test Bell's inequality using ballistic electrons in semiconductor nano-wires [6]. All these works are motivated by the promise of implementing Quantum Information Processing in solid-state setting. Many of these settings involve transport measurements across the sample that may include quantum dots or heterostructures. In both cases, basic quantum processes such as capture or emission of carriers and metastable states play a key role in understanding the measured current [7].

Condensed matter physics is another area that has been boosted by the possibility to observe different semiconductor phenomena in nano-structures such as the fractional Quantum Hall effect, the BCS-BEC crossover in semiconductor electron-hole bilayers [8], or Wigner crystallisation [9]. It is worth to mention that, any list of new semiconductor physics is incomplete since our understanding of low dimensional phenomena is influenced by what can be done in semiconductors.

In many cases, the phenomena mentioned above are put in evidence once an external magnetic field is applied. For example, the magnetic field is capable of shaping the electronic wave function in InAs quantum dot [10]. Nazmitdinov *et al.* showed that a given magnetic field induce shape transitions with symmetry changes in excited states of two-electron quantum dots [11], these transitions are also manifested as changes in an entanglement measure. Relatively small magnetic field strengths also modify the spectrum of excitons and electrons trapped in nano-wires [12, 13]. These effects are owed to two reasons. First, the small or very small effective mass of the electrons in most semiconductors leads to Landau levels radius at nanometer size with magnetic field strengths around tens of Teslas, therefor making possible to probe structures with characteristic length scales in the nanometer region. Second, the energy scale of electrons confined in a given structure is usually on the order of the tens of meV which, again, agrees with the energy scale of the Landau levels.

The stabilisation of metastable states due to the presence of magnetic fields was first analysed by Avron, Herbst and Simon [14], where they argued about the existence of negative Helium ions, a fact that was numerically tested very recently [15]. In atomic-like systems the field strengths necessary to show that the width of a resonance is zero are

Accepted Manuscript

about 10^5 Teslas [16]. Having this in mind, it is natural to ask if laboratory attainable magnetic fields strengths can bind few-electron resonant states in nano-devices. As early as in 1989, Sikorski *et al.* [17] found that the energies of electronic states in InSb quantum dots effectively depend on the magnetic field strength, but their study was restricted to low lying energy states of very deep quantum dots. This is remarkable, since the first clear evidence of discrete electronic states in semiconductor nanostructures was found a year earlier by Reed and co-workers [18].

The theoretical efforts to understand the phenomenon followed suit, Buczko and Bassani analysed the bound and resonant states of spherical GaAs/$Ga_{1-x}Al_xAs$ quantum dots [19], then Bylicki and W. Jaskólski [20] analysed the binding of one-electron resonances in a semiconductor quantum dot model. They found that the width of shape resonances were non-increasing functions of the magnetic field strength and that for large enough values the width become null. Resonance states of two-electron systems, without magnetic fields, were analysed in quantum dot [21] and atomic systems [22]. Also, the two-electron quasi-one-dimensional system was studied using entanglement quantities [23]. Sajeev and Moiseyev [24] demonstrated that the lifetime of resonance states of two-electron spherical quantum dots can be controlled by varying the confinement strength, Genkin and Lindroth reported that such control can be compromised by Coulomb impurities [25]. More recently, Ramos and Osenda [26] analysed the resonance states of one-electron cylindrical quantum dots with magnetic field using the fidelity and the localisation probability, *i.e.*, the probability that the electron is inside the potential well, to characterise the binding phenomenon.

It is well known that the binding of resonance states of two-electron quantum dots is harder to analyse than the one-electron problem, the main reason is the long-range and strength of the Coulomb repulsion between the electrons. Moreover, the system has a number of parameters that are all of significant importance, like the effective mass, characteristic lengths (whose number depends on the geometry of the quantum dot), the materials chosen to form the structure, strength of the magnetic field, among others. The magnetic field imposes an azimuthal symmetry, and assuming that the whole system has this symmetry leads, in many cases, to a simplified problem.

In this work we study the binding of resonance states of a two-electron cylindrical quantum dot embedded in a wire. In particular, we consider systems where the symmetry axis of the quantum dot, the wire and the magnetic field are collinear. We start with the well known one-electron case and we show that the problem can be treated using a modified strong-lateral-confinement approach and addressing the transversal problem in different ways it is possible to retrieve the binding (localisation) threshold with great accuracy and minimal effort. The strong lateral confinement approach presupposes that for certain few-electrons problems an approximate wave function can be constructed as the product of two functions [27], one that depends on the lateral (or radial) coordinates and other that depends on the longitudinal one. The accuracy of the coordinate disentanglement *ansatz* can be tested when the full three dimensional wave function is available. The disentanglement for the one electron problem is studied

Accepted Manuscript

using the von Neumann and purity of the reduced density matrices obtained tracing a coordinate from the full one-electron density matrix operator. This study provides a good understanding of the scenarios where the approximation better works. Later on, we study the two-electron problem using the modified strong lateral confinement approximation proposed for the one-electron problem and present a thorough analysis of the binding scenarios. We also show that the von Neumann entropy and the purity provide useful information to analyse the confinement of resonances. Finally, we discuss the actual implementation of an experiment setup, similar to the studied experimentally by Barettin *et al.*. [28].

The paper is organised as follows: In Section 2 the strong lateral confinement approximation is presented. In Section 3 the one-electron problem in three dimensions is analysed and we compare the three-dimensional results with the calculations using the strong lateral confinement approach. In Section 4 we propose a modified lateral confinement approximation. The Section 5 is devoted to the study of the two-electron problem in the modified lateral confinement approximation. Finally we discuss our findings and discuss about its implementation in actual experimental setups in Section 6.

2. Model and strong lateral confinement scenario

In what follows, we consider a two-electron cylindrical quantum dot, whose Hamiltonian is written in a single band effective mass approximation. The electrons are confined by a one-particle potential $V(\mathbf{r})$ and a constant magnetic field is applied along the axis of the quantum dot. Using the symmetrical gauge, the two-particle Hamiltonian is

$$H = h(1) + h(2) + W(1,2), \tag{1}$$

where $W(1,2)$ is the interaction between the electrons, and

$$h(j) = -\frac{\hbar^2}{2m_e^\star}\nabla_j^2 + V(\rho_j, z_j) + \frac{1}{2}m_e^\star\omega^2\rho_j^2 - i\hbar\omega\frac{\partial}{\partial\varphi_j}, \quad j = 1,2\,, \tag{2}$$

is the one-particle Hamiltonian in cylindrical coordinates, $m_e^\star$ is the effective mass of the electron, $\omega = eB/2m_e^\star c$ is the Larmor frequency, and we have put explicitly that the confining potential only depends on two coordinates: ρ and z. The spectrum of the Hamiltonian is obtained solving the eigenvalue equation

$$H\Phi(1,2) = E\Phi(1,2). \tag{3}$$

The one-electron Hamiltonian commutes with the angular momentum along the z-axis L_z, this means that the eigenvalues of this operator are good quantum numbers to label the one-electron Hamiltonian eigenfunctions. The same is true for the eigenfunctions of the two-electron Hamiltonian if the interaction between the electrons depends only on the interparticle distance. In this work, we focus on states with zero angular momentum along the z-axis for each electron.

The antisymmetry property of the two-electron system require that the two-electron wave function be antisymmetric under the exchange of the particle, *i.e.*

$$\Phi(1,2) = \Psi_{\substack{S\\A}}(1,2)\chi_{\substack{sing\\trip}}\,, \tag{4}$$

Accepted Manuscript

where $\Psi_{\substack{S\\A}}(1,2)$ is the symmetric (S) or antisymmetric (A) spatial wave function and $\chi_{\substack{sing\\trip}}$ is the singlet or triplet spin configuration. Since in bound two-electron systems the lowest eigenvalue corresponds to a singlet state, in this work we analyse symmetrical wave functions $\Psi(1,2)$, and drop the subindex S.

Following Bednarek [29], is reasonable to assume that the two-electron wave function, $\Psi(1,2)$, can be written as

$$\Psi(1,2) = R_{\perp}(\rho_1, \rho_2, \varphi_1, \varphi_2)\psi(z_1, z_2), \tag{5}$$

i.e. it is being assumed that the total wave function is *separable* in longitudinal and transversal coordinates. Afterwards, is it possible to obtain an effective one-dimensional two-particle Hamiltonian by introducing the *ansatz* Eq. (5) in Eq. (3) and integrating over the transversal coordinates ρ and φ, resulting in

$$H_{eff}(1,2)\psi(z_1, z_2) = E\psi(z_1, z_2)\,. \tag{6}$$

Some remarks are worthy to mention. First, once the separability assumption is made, the effective problem, Eq. (6), can be solved using different approaches. Two, the solution in Eq. (5) can be thought as a variational trial function, so the lowest eigenvalue of Eq. (6) is an upper bound for the ground state energy. Third, the one-particle effective Hamiltonians are tractable with a host of different choices for the transversal function, regrettably, the interaction term is more involved. Bednarek *et al.* chose as the transversal function the product of the ground state wave functions of two harmonic oscillators, $R_{\perp} = \phi_0(\rho_1)\phi_0(\rho_2)$, which leads to an analytical expression for the effective Coulomb interaction, for details see [29].

So far, we have made no explicit choice of the one-particle confining potential since, up to this point, the analysis does not depend on its particular shape. In Section 3 we restrict our analysis to a particular potential and consider the one-electron problem only.

3. One-electron problem

Here, and in what follows, we consider the confining potential given by

$$V(\rho, z) = \begin{cases} -V_0 & \text{if} \quad \rho \le a_\rho \quad \text{and} \quad |z| \le a_z/2 \\ V_1 & \text{if} \quad a_z/2 \le |z| \le (a_z + b_z)/2 \\ 0 & \text{otherwise} \end{cases} \tag{7}$$

i.e., is a cylindrical potential well of length a_z, radius a_ρ and depth $-V_0$ limited by two infinite plane slabs of height V_1 that are perpendicular to the cylinder axis. The width of both slabs is $b_z/2$. Figure 1 shows the schematic structure which generates the potential given in Eq. (7). For adequately chosen parameters the one-electron problem has no bound states for $B = 0$, this means that the spectrum of the one-electron Hamiltonian is continuous and all the eigenfunctions are extended ones. However there might be isolated eigenvalues embedded in the continuous spectrum that correspond to localised eigenfunctions with outgoing boundary conditions which are called resonant

Accepted Manuscript

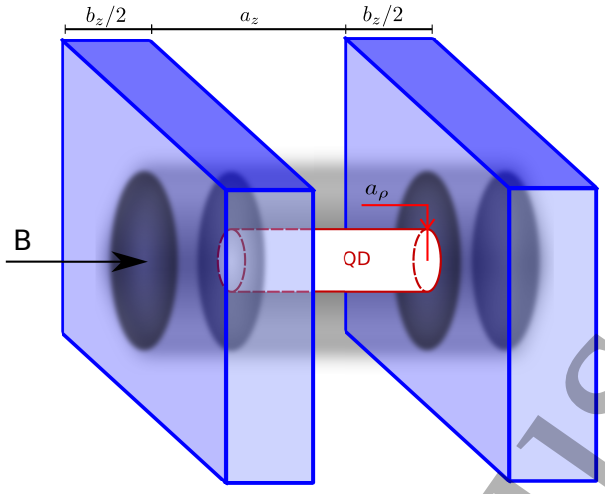

Figure 1. Schematic structure of the cylindrical quantum dot (white cylinder). The blue parallelepipeds are two slabs made of a semiconductor different from the one from which the quantum dot is made of. The grey shaded areas represent the confining effect of the applied magnetic field.

states [32]. In the setups we studied, the one-electron system has only one low lying resonant state for $B = 0$, which have been studied in Ref. [26]. We first intend to clarify some issues, namely if a separable ansatz, like the one in Eq. (5), could provide an accurate value for the lowest eigenvalue of the Hamiltonian and what physical traits of the three-dimensional problem are well described by the one-dimensional one.

The eigenvalue problems in this section, and in the whole work, were solved implementing a high-precision variational approach using basis functions known as B-splines. The B-spline functions can be used efficiently in calculations of multivariable problems like two-electron atomic systems or two-dimensional systems [30]. Every particular problem, *i.e.*, one- or two-electron in one or three dimensions, needs a specific basis set suitable to it that has the proper symmetries and boundary conditions. In Appendix A we describe the basis sets used in the problems of the present and the following sections.

Figure 2 shows the lowest approximate energies of the one-electron problem as functions of the magnetic field strength. For illustrative purposes we use an effective mass $m^\star = 0.041 m_e$ corresponding to $Ga_{0.47}In_{0.53}As$, a commonly used material to define quantum dots inside a GaAs matrix [31]. The quantum dot chosen parameters are $a_\rho = 7\,nm$, $a_z = 7\,nm$, $b_z = 2.5\,nm$, $V_1 = 0.37\,eV$, $V_0 = 0.10884\,eV$. There are, at least, two salient features in the curves shown. First, the lowest eigenvalue crosses the energy of the lowest Landau level (the red dashed line) for a critical field $B_c \approx 17T$. Second, above the lowest Landau level (LLL), the density of states shows a remarkable increase, pointing to the existence of a threshold. In Ref. [26] these features were analysed thoroughly. Here, we include the spectrum to point that in the presence of the magnetic field the energy of the LLL is the threshold that separates the bound isolated

Accepted Manuscript

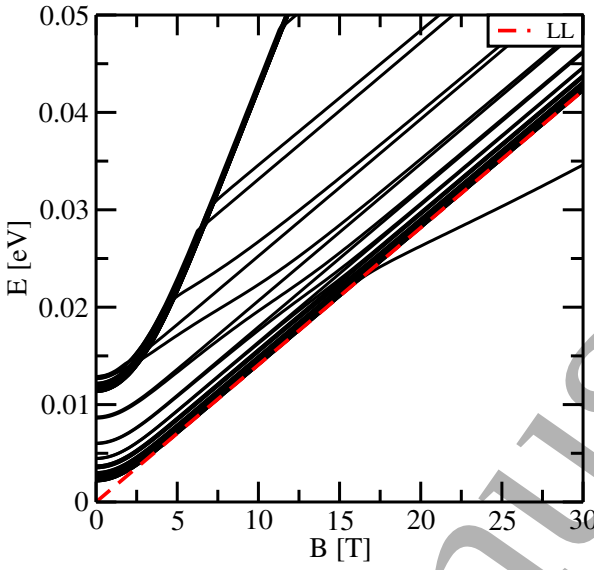

Figure 2. Lowest approximate energies as a function of magnetic field strength for one-electron confined in a cylindrical quantum dot defined by Eq. (7). The red dashed line is the lowest Landau level energy $\hbar\omega$. Notice the increase in the density of eigenvalues for $E(B) > \hbar\omega$ and the stabilisation of some continuum eigenvalues that evidences the presence of the resonance energy.

state from the continuum of extended ones, simply because the energy of the electron far away from the quantum dot is $\hbar\omega$. In other words, the magnetic field strength $B^\star$ where the lowest eigenvalue $E_0(B^\star)$ crosses the LLL signals the resonance binding. If one analyses the behaviour of the lowest energy for decreasing field strengths, then the energy of the resonance for $B < B^\star$ is the analytical continuation of the lowest eigenvalue when it enters into the continuum. Inversely, for increasing field strength, the resonance mean lifetime diverges at $B = B^\star$ and becomes a stable bound state for $B > B^\star$. That is, for our setup with no bound states at $B = 0$, the presence of an isolated eigenvalue below the threshold is more than enough to mark the binding of a resonance and is the signal that we will be looking for when we deal with the two electron problem. Nevertheless, there are several other ways to identify the binding scenario besides the calculation of the resonance width (using, for example, exterior complex scaling [32]). In Ref [26] the fidelity [33] and the localisation probability were also used.

We are interested in resolving for which cases the strong lateral confinement gives a good approximation of the ground state wave function. In order to do this we analyse the purity [34], the von Neumann entropy and the radial density. The purity and the von Neumann entropy are commonly used to asses if a given quantum state is pure of mixed. Here we are dealing, so far, with the one-electron problem, and thus the partition of the system is made on the coordinates.

For a bipartite pure quantum state, $|\chi(1,2)\rangle$, the purity is defined by

$$p = \mathrm{Tr}(\rho_1^2), \quad \text{where} \quad \rho_1 = \mathrm{Tr}_2(|\chi(1,2)\rangle\langle\chi(1,2)|), \tag{8}$$

Accepted Manuscript

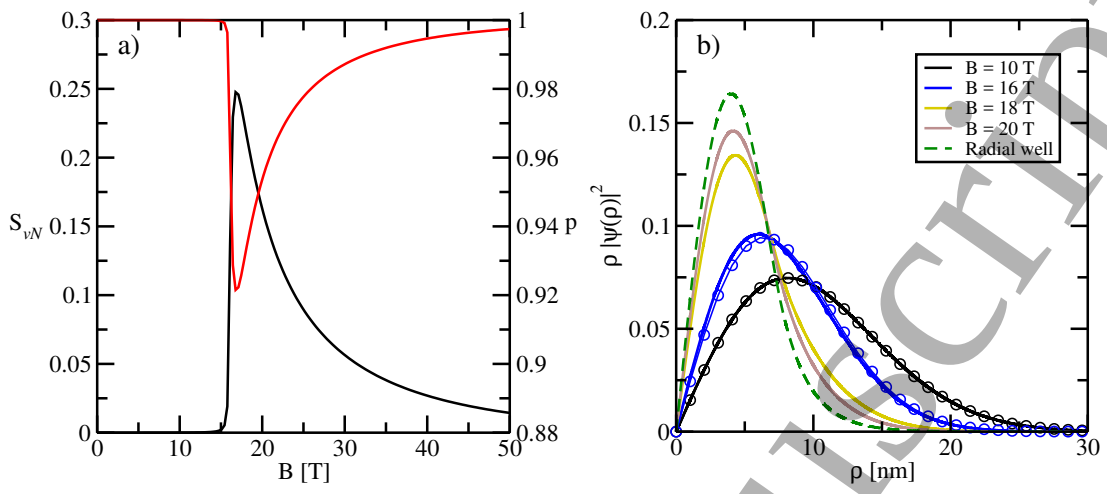

Figure 3. (a) The purity p (red solid) and von Neumann entropy (black solid) for the ground state of an electron in a quantum dot as functions of the magnetic field strength B. The critical field is about $B^\star \approx 17$T. For $B < B^\star$ the purity is one, which means that the three-dimensional wave function is separable in ρ and z coordinates. Accordingly, the von Neumann entropy vanishes. If the magnetic field is large enough, the purity goes also to unity. For $B \gtrsim B^\star$, both quantifiers indicate an increase in correlation as we approach the critical field $B^\star$. (b) Radial density (RD) for different values of the magnetic field strength B. The solid lines correspond to the RDs obtained from the variational ground state wave function ($B = 10, 16, 18, 20$). The RDs for the LLLs are depicted with empty circles ($B = 10, 16$) and the green dashed line is the exact RD for the radial well potential of Eq. (13). Note that for $B < B^\star$ the variational RD is quite similar to the RD of the Landau levels and, conversely, it approaches to the exact RD the radial well for $B > B^\star$.

where ρ_1 is the reduced density operator, and the purity is the sum of its eigenvalues squared. The von Neumann entropy is also defined by the reduced density operator by

$$S_{vN} = -\mathrm{Tr}(\rho_1 \log_2(\rho_1)) \,, \tag{9}$$

From the variational eigenfunction that corresponds to the lowest eigenvalue, $\psi^v(\rho, z)$, two reduced density operators can be obtained

$$\delta(z, z') = \int (\psi^v(\rho, z))^\star \, \psi^v(\rho, z') \, \rho \, d\rho, \tag{10}$$

and

$$\delta(\rho, \rho') = \int (\psi^v(\rho, z))^\star \, \psi^v(\rho', z) \, dz. \tag{11}$$

In Appendix A it is shown how to calculate these quantities, reduced density operators, purity and von Neumann entropy, using a variational wave function.

The operators $\delta(z, z')$ and $\delta(\rho, \rho')$ are different but both have the same spectrum, as it is for any bipartite pure state. This means that the information content obtained from the reduced density matrix in the coordinate z is the same as the one obtained from the reduced density matrix in the coordinate ρ.

Accepted Manuscript

Figure 3(a) shows the behaviour of the purity and the von Neumann entropy as a function of the magnetic field strength. Both quantities show the same scenario: up to the critical value $B^\star$ the wave function ψ^v is a product of two functions that depend, separately, on the coordinates ρ and z

$$\psi^v \simeq f(\rho)g(z)\,. \tag{12}$$

For large enough values of B the wave function becomes, again, a product of two functions, one that depends only on ρ and the other one only on z. There is an intermediate region where a separable function like Eq. (12) is a poor approximation to ψ^v.

Figure 3(b) shows the radial density for different values of the magnetic field strength, as functions of the radial coordinate. Again, the transition from extended states to localised ones is manifested, in this case by the abrupt change in the shape of the functions. Furthermore, for values of $B < B^\star$ the shape of the radial density is quite similar to the radial density of the Landau Level, while for values of $B \gtrsim B^\star$ the shape of radial density looks like the radial density of the exact wave function of a two-dimensional well, V_{2D}, with parameters equal to the ones on the three-dimensional one

$$V_{2D}(\rho) = \begin{cases} -V_0 & \text{if} \quad \rho \leq a_\rho \\ 0 & \text{otherwise} \end{cases}. \tag{13}$$

If we increase the field even further, $B \gg B^\star$, we recover again the LLL shape and the radial density is again dominated by the field because the Landau radius is smaller than a_ρ.

The findings described above leads us to study different approaches for the longitudinal eigenvalue problem

$$H_z\psi_z(z) = \langle R(\rho)|H|R(\rho)\rangle\psi_z(z) = E\psi_z(z), \tag{14}$$

where $R(\rho)$ is some normalised function. The analysis of the data in Figures 2 and 3 suggests two possible choices, $R(\rho) = \psi_{2D}(\rho)$ (see Appendix B) and

$$R(\rho) = \psi_{LLL}(\rho) = \sqrt{\frac{2m_e\omega}{\hbar}}\, e^{-\frac{m_e\omega}{\hbar}\rho^2/2}\,. \tag{15}$$

The potential in the longitudinal Hamiltonian, Eq. (14), is constructed in terms of the chosen radial function

$$V(z) = \langle R(\rho)|V(\rho,z)|R(\rho)\rangle = \begin{cases} -V_0V_R & \text{if} \quad \rho \leq a_\rho \quad \text{and} \quad |z| \leq a_z/2 \\ V_1 & \text{if} \quad a_z/2 \leq |z| \leq (a_z/2 + b_z)/2 \\ 0 & \text{otherwise} \end{cases} \tag{16}$$

where

$$V_R = \int_0^{a_\rho} |R(\rho)|^2 \rho\, d\rho. \tag{17}$$

The spectrum of the longitudinal Hamiltonian is also calculated numerically using a variational approach that employs B-spline functions.

Accepted Manuscript

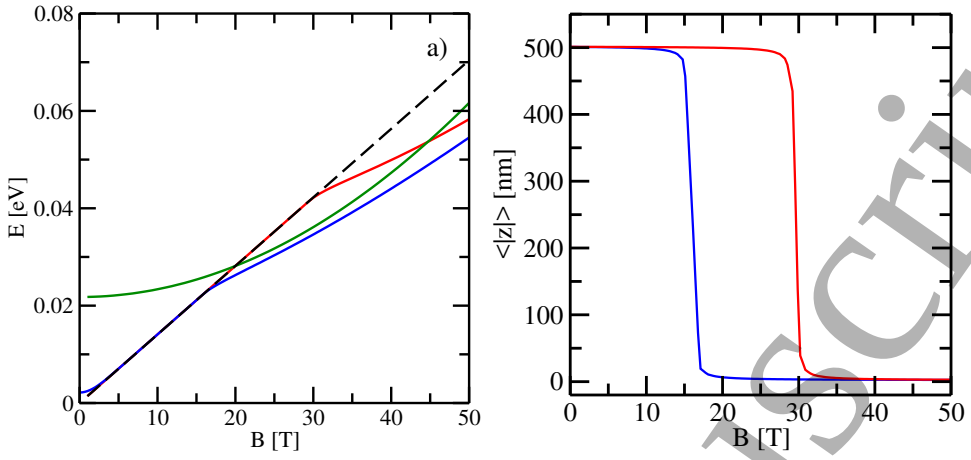

Figure 4. (a) Lowest eigenvalue obtained for the one-particle three-dimensional problem (blue solid), for the longitudinal problem defined using $R(\rho) = \psi_{2D}(\rho)$ (green solid) and for the one defined using $R(\rho) = \psi_{LLL}(\rho)$ (red solid). The black dashed line is $\hbar\omega$. (b) Expectation value of the absolute value of the z-coordinate for the one-particle three-dimensional problem (blue solid) and for the longitudinal problem defined using $R(\rho) = \psi_{LLL}(\rho)$ (red solid).

Figure 4 (a) shows the lowest eigenvalue obtained for the one-particle three-dimensional problem (blue solid line), for the longitudinal problem defined using $R(\rho) = \psi_{2D}(\rho)$ (green solid line) and for the one defined using $R(\rho) = \psi_{LLL}(\rho)$ (red solid line), in all cases as a function of the magnetic field strength. The ground state energy for the Landau levels corresponds to the black dashed line. It is clear that each approximation has its advantages and disadvantages. The longitudinal problem constructed using $\psi_{2D}(\rho)$ gives a very good approximation to the critical field where the binding happens, and from $\approx 20T$ up to $\approx 45T$ it also gives a better approximation to the eigenvalue of the three-dimensional problem. On the other hand, the curve does not show any change in its behaviour near the threshold, so without further information this approach does not offer a way to identify that the eigenvalue has crossed the binding threshold.

The lowest eigenvalue, E_{gs}^{LL}, obtained using lateral confinement approximation with the LLL as a lateral wave function, shows a well defined change in its behaviour. If $B \lesssim 30T$, E_{gs}^{LL} follows closely the energy of the LLL, E_{LLL}, for $B > 30T$ it is always smaller than E_{LLL}, and for large enough values of B, both curves become parallel. So, the qualitative behaviour is correct, but the upper bound to the binding field $B^{\star}$ is not close to the 3D estimation (an error of $\approx 15T$).

The change in the shape of the wave function for B values below or above the binding field is depicted in figure 4 (b). The expectation value of $|z|$ clearly shows that the state is localised inside the quantum dot for fields above the binding one.

From what has been stated in the previous paragraphs, it is clear that it is necessary to modify the way in which the strong lateral confinement approximation is made,

Accepted Manuscript

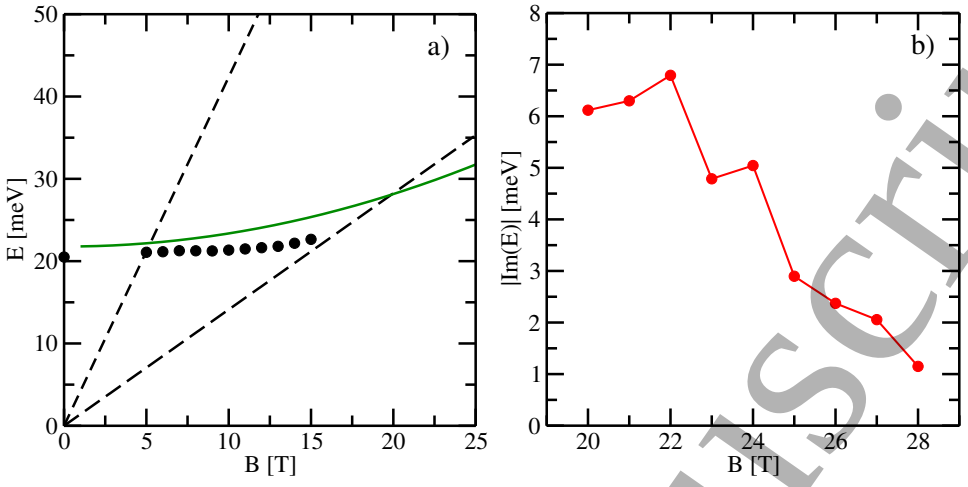

Figure 5. (a) Comparison between the real part of the resonance energy (black dots) calculated with complex exterior scaling and the lowest eigenvalue (green solid) of the lateral confinement approximation with $\psi_{2D}(\rho)$ as radial wave function. The two black dashed lines are the energies of the two first Landau levels with null angular momentum. (b) Imaginary part of resonance energy obtained using complex exterior scaling in the lateral confinement approximation with $\psi_{LLL}(\rho)$ as radial wave function.

so the resulting longitudinal problem is able to provide a good approximation of the lowest three-dimensional eigenvalue before and after the binding takes place. But before introducing such modification (section 4), we want to discuss the meaning of the lowest eigenvalue of the longitudinal problem obtained for $B < B^{\star}$ using $R(\rho) = \psi_{2D}(\rho)$.

One of the basic assumptions that support our work is that the energy of the localised state that appears below the threshold, in our case the energy of the LLL, is the analytical continuation of the complex energy of resonance state. So, it is reasonable to think that choosing $\psi_{2D}(\rho)$ as the radial wave function in the lateral confinement approximation, we could get a good approximation to the real part of the resonance state energy in the continuum region.

Figure 5 (a) shows the lowest eigenvalue for the longitudinal problem defined by $\psi_{2D}(\rho)$ (green solid line), the first two Landau levels with null angular momentum and data calculated using a high-precision variational complex exterior scaling (black dots), see References [26, 35]. The basis set used to obtain the data shown as dots had up to 3600 functions. The agreement between the energies obtained using the two methods is surprisingly good taking into account the quite different amounts of numerical work involved in one method and the other. The energy difference between the two sets of data is due to the approximation in the longitudinal approach in which we assume a separable wave function in the coordinates for a correlated three-dimensional Hamiltonian.

As was stated before, the longitudinal problem defined by the radial function $\psi_{2D}(\rho)$ gives a good approximation of the real part of the resonance energy in the continuum region, but the lowest eigenvalue of this problem does not show any change in its behaviour revealing the binding phenomenon. However, the longitudinal problem

Accepted Manuscript

with $\psi_{LLL}(\rho)$ as radial wave function does it (the derivative of the eigenvalue shows a discontinuity), so it is possible to obtain the imaginary part of the resonance energy, or width of the resonance state, applying the exterior complex scaling method [32]. This method consist in rotating the coordinate outside a given length, z_0, into the complex plane

$$z = \begin{cases} z' & \text{if } |z'| < z_0 \\ z'\, e^{i\theta} & \text{if } |z'| \geq z_0 \end{cases} , \tag{18}$$

where θ is the rotation angle and we choose z_0 as the coordinate where the confinement potential become null, in our case this value is $z_0 = 5\,nm$. With this choice only the kinetic term of the Hamiltonian is rotated in the complex plane. The resonance width obtained following the prescription described above is shown in Figure 5(b), where it can be observed that the width of the resonance goes to zero when the magnetic field strength increases. The width values shown in the figure are consistent with those obtained using other method [26], despite the simplification imposed by the strong lateral confinement assumption.

4. One-electron problem: modified lateral confinement method

As shown in Figure 4, the lowest eigenvalue of the three dimensional problem and the lowest eigenvalue of the longitudinal problem defined by $\psi_{LLL}(\rho)$ behave similarly for small or very large fields strengths. So, it is tempting to modify the procedure to obtain a better one-dimensional approximation when the radial function is $\psi_{LLL}(\rho)$. The main reason to maintain $\psi_{LLL}(\rho)$ as the radial wave function is that, as Bednarek *et al.* [29] have shown, it provides a systematic way to deal with the Coulomb repulsion between electrons. Based on the results of [26], concerning the expectation value of the coordinate z and the probability of localisation, we can assure that the bound isolated state is localised inside the potential well. Moreover, since the radial densities shown in figure 3(b), for $B > B^{\star}$, show no contribution outside the well radius, we can assume that the density over the barrier is also radially confined. Then, in the longitudinal approximation, we propose that the one-dimensional potential is given by

$$V_{long}(z) = \begin{cases} -V_0 V_R & \text{if} \quad |z| \leq a_z/2 \\ V_1 V_R & \text{if} \quad a_z < |z| \leq (a_z + b_z)/2 \\ 0 & \text{if} \quad \text{otherwise} \end{cases} . \tag{19}$$

Figure 6 shows the lowest eigenvalue, as functions of the magnetic field strength, for different configurations of the potential. The eigenvalues were calculated for the full three-dimensional problem (solid lines) and for the one-dimensional Hamiltonian Eq. (14) (empty symbols).

The agreement between both sets of eigenvalues is remarkable, and the approximation seems to work very well for a broad set of parameters, mainly for potential wells such that $a_\rho \lesssim a_z$. Here we want to point that there is a drawback in this approach,

Accepted Manuscript

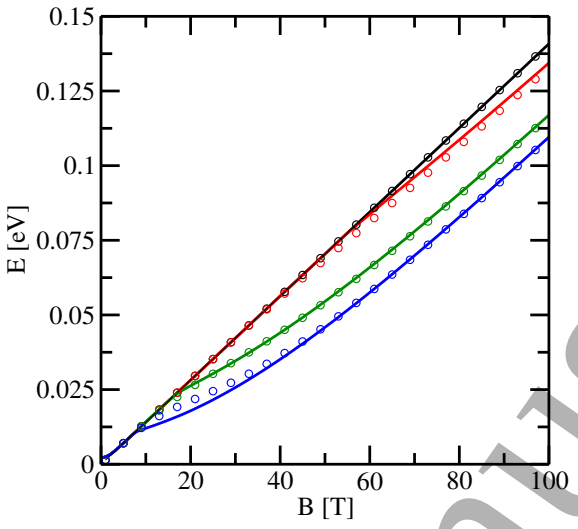

Figure 6. Lowest eigenvalue for the three-dimensional one electron problem (solid line) and the corresponding lowest eigenvalue for the effective one-dimensional problem within the modified lateral confinement approximation (empty circle). The height of the barrier and the deep of the well are the same as 4, the with of the barrier is $b_z = 2.5\,nm$. The data in black is for $a_\rho = a_z = 5\,nm$, the red data is for $a_\rho = a_z = 6\,nm$, the green data is for $a_\rho = a_z = 7\,nm$ and the blue data is for $a_\rho = a_z = 7.5\,nm$.

the modification of the potential barrier results in a non-variational approximation for the eigenvalues, so the eigenvalues obtained with the Hamiltonian in Eq. (14) can be, near the threshold, larger or smaller than their three-dimensional counterparts. Despite this, since it is the best available one-dimensional approximation we will use it to study the binding of two interacting electrons in the same potential well.

5. Two-electron problem

One of the advantages of assuming a separable wave function as in Eq. (5) is evidenced when the effective interaction is calculated. Specifically, using for the confinement function

$$R_\perp(\rho_1, \rho_2) = \phi_0(\rho_1)\phi_0(\rho_2), \tag{20}$$

where ϕ_0 is some radial function that can be chosen at convenience. Since we are interested in the singlet spin configuration, the spatial wave function must be totally symmetric under particle exchange. Because $R_\perp(\rho_1, \rho_2)$ is symmetric, we compute only the symmetrised solutions $\psi(z_1, z_2)$. Since the effective one-dimensional interaction, $W_{eff}(z_1, z_2)$, is defined as

$$W_{eff}(z_1, z_2) = \int d\rho_1 \int d\rho_2 \, |R(\rho_1, \rho_2)|^2 W(1,2)\rho_1\rho_2 \,, \tag{21}$$

Accepted Manuscript

where $W(1,2)$ is the full three-dimensional interaction between the electrons, it is clear that only a handful of choices for ϕ_0 result in an analytical expression for the effective interaction. Fortunately, this is the case when $\phi_0 = \psi_{LLL}$ and the interaction is given by the Yukawa (or Coulomb screened potential) potential

$$W^{\alpha}(1,2) = \frac{e^{-\alpha|\mathbf{r}_1-\mathbf{r}_2|}}{|\mathbf{r}_1-\mathbf{r}_2|}. \tag{22}$$

Here α is a constant and the, more usual, Coulomb potential case is obtained taking the limit $\alpha \to 0$.

Using the Fourier transform expressions of Eqs. (20) and (22), and after some algebra, it is shown that

$$W_{eff}(z_1,z_2) = V_{eff}(|z_1-z_2|) = e^{x^2+y^2}\sqrt{\frac{\pi}{2}}\frac{1}{\ell}(1-erf(x+y)), \tag{23}$$

where $erf(x)$ is the error function [36],

$$x = \frac{|z_1-z_2|}{\sqrt{2}\ell}, \quad y = \frac{\alpha\ell}{\sqrt{2}} \quad \text{and} \quad \ell = \sqrt{\frac{\hbar}{m_e^{\star}\omega}}, \tag{24}$$

see Ref. [29] for more details.

In the Coulomb case ($\alpha = 0$), the asymptotic limits of V_{eff} can be obtained straightforwardly. For $x \longrightarrow \infty$

$$V_{eff} \approx \frac{1}{|z_1-z_2|} - \frac{\ell^2}{|z_1-z_2|^3} + \ldots, \tag{25}$$

and, for $x \longrightarrow 0$,

$$V_{eff} \approx \frac{1}{\ell}\sqrt{\frac{\pi}{2}} - \frac{|z_1-z_2|}{\ell^2} + \ldots. \tag{26}$$

Clearly the Coulomb limit is obtained for $x \to \infty$ and, more interestingly, the $x \to 0$ relates the inverse transversal size l with the contact value ($z_1 = z_2$) of the potential.

Given the asymptotic limits of V_{eff}, Eqs. (25) and (26), it is customary in setups that produce almost one-dimensional behaviour [37, 38] or strong lateral confinement [39], to use the following interaction potential

$$V_{rec}(z_1-z_2) = \frac{1}{\sqrt{|z_1-z_2|^2+d^2}}, \tag{27}$$

where η and d are constants. It is clear that the potential in Eq. (27) has the same asymptotic behaviour than V_{eff}. The short distance cutoff d is chosen to be much smaller than the characteristic confinement length of the system [38], in particular we take $d = 0.1\ nm$ since in our setups $a_\rho, a_z \approx 10\ nm$.

Summing up, after all the consideration made, the two-particle one-dimensional Hamiltonian can be written as

$$H_z = 2\hbar\omega - \frac{\hbar^2}{2m_e^{\star}}\left(\frac{\partial^2}{\partial z_1^2} + \frac{\partial^2}{\partial z_2^2}\right) + V_{long}(z_1) + V_{long}(z_2) + W_{long}(z_1,z_2), \tag{28}$$

Accepted Manuscript

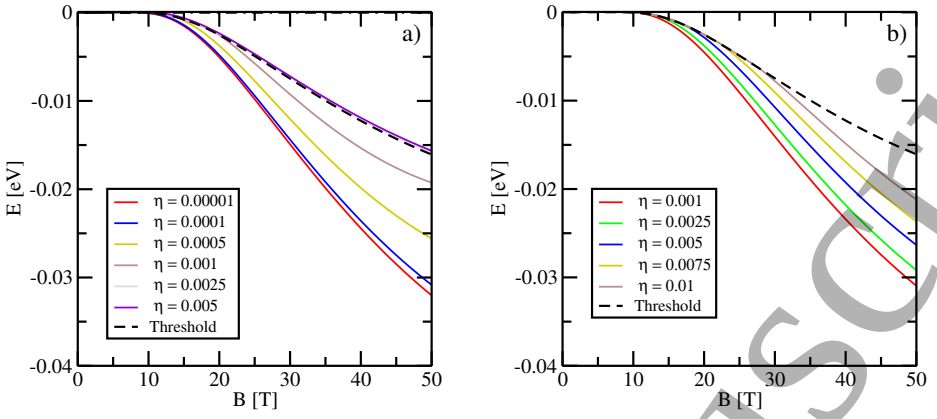

Figure 7. Difference between the lowest eigenvalue of the Hamiltonian (6) and the energy of the LLL for two non-interacting electron, $2\hbar\omega$. The black dashed line is the one-electron threshold. (a) eigenvalue of the two-electron problem with the effective Coulomb interaction Eq. (23) and (b) eigenvalue of the two-electron problem with the rectified Coulomb interaction Eq. (27). Units of η are $1\ Ha \times a_0$, where a_0 is the Bohr radius.

where $V_{long}(z)$ has been defined previously, Eq. (19), and there are two possible choices to the interaction term, one is

$$W_{long}(z_1, z_2) = \eta\, V_{eff}(|z_1 - z_2|), \tag{29}$$

and the other one is

$$W_{long}(z_1, z_2) = \eta\, V_{rec}(|z_1 - z_2|). \tag{30}$$

In typical semiconductors the Coulomb repulsion energy between two electrons confined in a region with a characteristic length of 10 nm is on the order of 5 meV. Accordingly, we chose η values in the order of 0.01 $nm\ eV$. Figure 7(a) shows the lowest eigenvalue calculated for the two-particle Hamiltonian, Eq. (28), with the effective Coulomb potential, Eq. (29), while figure 7(b) shows the eigenvalue calculated with the interaction term given by Eq. (30).

Both panels in figure 7 show the binding threshold as a black dashed line. They always are defined as the ground state energy of the one-electron system. For $B < B^\star$ it is defined by twice the LLL energy $2\hbar\omega$. For $B > B^\star$ the system binds one electron to the quantum dot and then the threshold can be written as $\hbar\omega + E^1_{bind}(B)$, where $E^1_{bind}(B)$ is the energy of one electron once it is bound. Both figures show that for small enough values of the effective charge η, the system shows two-electron resonance binding. Moreover, the binding is found for values of the magnetic field strength similar to the one necessary to bind one-electron resonances, $B^\star$. There are, however, intermediate values of η for which the binding of the two-electron resonance occurs for $B^\star_{2e} > B^\star$, and for these values the two electron bound state is detached from the bound one-electron threshold.

Accepted Manuscript

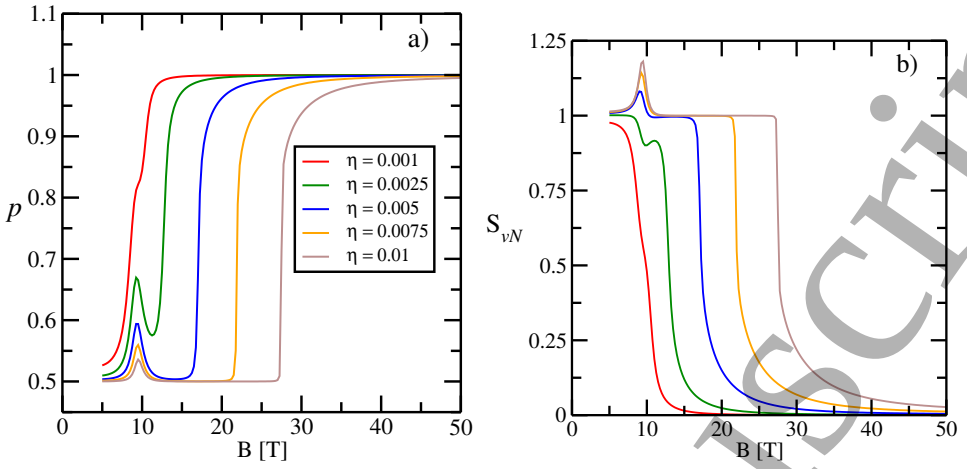

Figure 8. The purity and the von Neumann entropy, panels (a) and (b) respectively, for the two-electron rectified model. The colour scheme corresponds to the data shown in figure 7(b). (a) The purity $p \approx 1$ when the state is localised and its value drops more or less abruptly when the energy eigenvalue become equal to the one-electron binding threshold. The peak that can be observed around $B \approx 10T$ manifests that the eigenvalue has a value equal to energy of the LLL for that field. (b) The von Neumann entropy shows a behaviour complementary to the observed by the purity, when the state is localised the von Neumann entropy value is quite small, it grows abruptly when the magnetic field strength decreases and the energy eigenvalue crosses the localisation threshold.

The localisation process of the lowest two-electron state involves the crossing of two thresholds by its energy eigenvalue when the magnetic field is increased: one is the LLL energy and the other is the one-electron binding energy. These crossings are manifested by the behaviour of the von Neumann entropy and the purity of the corresponding state. In figure 8 it is shown the behaviour of both quantities as functions of the magnetic field strength B, for the rectified model. Figure 8 employs the same colouring convention that is used in figure 7 and the von Neumann entropy is calculated tracing out one particle of the two-particle density matrix. Figure 8(a) shows that for a given value of the parameter η, for instance $\eta = 0.01$, $p \approx \frac{1}{2}$ for small fields, around $B \approx 10T$ it shows a well defined peak, it becomes again approximately equal to one half and then it grows abruptly up to $p \approx 1$. The peak precedes the value of $B^\star$ where the energy eigenvalue (shown in figure 7(b)) crosses the energy of the LLL, while the abrupt growing starts exactly where it crosses the one-electron binding energy. For smaller values of η, like $\eta = 0.001$, the peak and the abrupt growing overlap and the peak disappears. This is attributed the weak interaction between the electrons since the localisation of both of them occurs at $B^\star$ and then is driven by the one electron properties.

The von Neumann entropy, as shown in figure 8(b), provides a complementary description of the binding process. When the state is localised the von Neumann entropy is very small, while for extended states its value is close to the unity. Again, near $B \approx 10T$ there is a change on its behaviour attributable to the closeness between the

Accepted Manuscript

two-electron energy eigenvalue and the energy of the LLL.

6. Conclusions and discussion

Tuning the energy of a resonance state in nanostructures can lead to a better performance of the task for what the underlying device was built for, or, what is even more interesting, to widen the functionalities of the device. Here we show that the magnetic field confinement allows binding and localisation of one- and two-electron resonances in cylindrical semiconductor quantum dots, a change in the nature of the states (from metastable to bound) that strongly affects, for example, the optical properties.

Previous studies in atoms [15] and in quantum dots [20, 26] pointed that, in the case of bound states, there is a localisation phenomenon along the magnetic field axis and also that the binding energy of the state is an increasing function of the magnetic field strength. In the case of shape resonances of one electron systems, they were shown to become more stable for increasing field strengths and eventually become bound after a critical field. Here we point that two-electron resonances show also localisation and binding in quantum dots, and that both increase with the field strength.

The two-electron system, in distinction to the one-electron case, can have different thresholds because the one-electron system can have resonance binding as well. The resonances that become bound for increasing magnetic fields may cross the one- or zero-electron threshold, according to the strength of the electron-electron interaction. However, we note that the crossing of the zero-electron threshold can occur only at the same critical field $B^\star$ as the one-electron case, because the electron-electron interaction is repulsive. This allows much more richer tuning possibilities, as the near threshold behaviour of the two-electron system is expected to be quite different for the two scenarios. For example, the two-electron wave function is expected to maintain localisation as it approaches the one-electron threshold, but it may not be the case if it crosses the zero-electron threshold. Further work on this area is needed to answer this question, that can certainly influence, for example, the optical properties of the quantum dot.

We implemented a simple and tractable approximation based on effective potentials to solve the one-electron problem. The scheme, based on geometrical considerations, leads to good approximations to the exact three-dimensional energies in the resonance and bound regions. We found that, the binding critical field $B^\star$ is properly described if we limit the whole potential felt by the electron to only the region where its wave function is expected to be different from zero. These simplifications allows to construct a simple effective model for the two-electron case that shows the correct qualitative resonance binding phenomena.

Barettin *et al.* [28] have recently implemented a nano-structure that strongly resembles our setups. The sizes and energies are quite close to the ones we used to obtain the resonance binding, but for the height of the potential barrier. With their

Accepted Manuscript

sizes and materials there is a host of bound states inside the dot at zero field, which makes the resonance binding scenario more difficult to analyse. To achieve our scenario, where is no bound states at zero field, the radius of the quantum dot should be strongly reduced, from 20 nm to ≈ 1 nm, but this increases the critical field necessary to bind the resonance. This can be avoided either by using different materials or using electrostatic gates to enhance the barrier heights.

Acknowledgments

We acknowledge SECYT-UNC and CONICET for partial financial support. We would like to thank A. Ramos for providing us with the data [35] of the resonance energies included in figure 5.

Appendix A. Method

The B-splines are functions designed to generalise polynomials for the purpose of approximating arbitrary functions. A complete description of B-splines and their properties can be found in the book [40]. A family of B-spline functions, $B_i^{(k)}(x)$, $i = 1, ..., n$ is completely defined given $k > 0$, $n > 0$, a sequence of knots $\mathbf{t} = \{t_i\}_{i=1,...,n+k}$ and the recursion relation given by,

$$B_i^{(1)}(x) = \begin{cases} 1 & \text{if} \quad t_i \leq x < t_{i+1} \\ 0 & \text{otherwise,} \end{cases} , \tag{A.1}$$

$$B_i^{(k)}(x) = \frac{x - t_i}{t_{i+k-1} - t_i} B_i^{(k-1)}(x) + \frac{t_{i+k} - x}{t_{i+k} - t_{i+1}} B_{i+1}^{(k-1)}(x) . \tag{A.2}$$

Each $B_i^{(k)}(x)$ is defined over and interval $[t_i, t_{i+k}]$, which contains $k + 1$ consecutive knots, and it is indexed by the knot where it starts.

The B-spline basis functions is widely used in quantum mechanical systems. A detailed description of the B-splines functions and their numerical implementation in quantum problems are shown in [30], here we show the different basis set used in the problems of this work.

We start with the three-dimensional case. We study the states with zero angular momentum, so each basis function, in cylindrical coordinates, is given by,

$$|\phi_{i,j}^{3D}(\rho, z)\rangle = C_{i,j}\, B_i^{(k_\rho)}(\rho)\, B_j^{(k_z)}(z) , \tag{A.3}$$

where $C_{i,j}$ is the normalisation constant and we chose different order for the B-splines in each coordinate. Also we have two knots sequence, one for each coordinate. For the variable ρ the uniform sequence was chosen in the interval $[0, R_{max}]$ with $R_{max} = 50\, nm$, and the exponential knot sequence for the variable z in the interval $[Z_{min}, Z_{max}]$ with $Z_{max} = -Z_{min} = 100\, nm$.

Accepted Manuscript

For the problem of one electron in the strong lateral confinement approximation the chosen basis functions are,

$$|\phi_i^{1D}(z)\rangle = \hat{C}_i\, B_i(z)\,, \tag{A.4}$$

where $\hat{C}_i$ is the normalisation constant. In this case we use the same knot distribution and the same interval as the used for the z coordinate in the three-dimensional problem.

Finally, for the two-electron problem within the lateral confinement approximation we solve the eigenvalue problem for symmetric states, so the matrix element of the Hamiltonian, Eq. (6), are calculated in the basis,

$$|\Phi_{i,j}\rangle = \begin{cases} \frac{|\phi_i^{1D}(z_1)\rangle|\phi_j^{1D}(z_2)\rangle + |\phi_i^{1D}(z_2)\rangle|\phi_j^{1D}(z_1)\rangle}{\sqrt{2}} & \text{if} \quad i \neq j \\ |\phi_i^{1D}(z_1)\rangle|\phi_j^{1D}(z_2)\rangle & \text{if} \quad i = j \end{cases}, \tag{A.5}$$

where z_j is the coordinate of the electron $j = 1, 2$. Here we use, again, a exponential distribution for the knots, but the limits of the interval are $Z_{max} = -Z_{min} = 1000\, nm$, in this way we ensure that the wave function satisfy the boundary condition.

Now we focus on how to calculate the purity and the von Neumann entropy when the wave function was obtained using the variational method. The following applies either for the one-electron three-dimensional problem and for the two-electron one-dimensional problem.

For a bipartite pure quantum state, $|\Psi(1,2)\rangle$, the purity and the von Neumann entropy are given by

$$p = \mathrm{Tr}(\rho_1^2)\,, \quad S_{vN} = -\mathrm{Tr}(\rho_1 \log_2(\rho_1))\,, \tag{A.6}$$

where $\rho_1 = \mathrm{Tr}_2(|\Psi(1,2)\rangle\langle\Psi(1,2)|$, is the reduced density operator. It is important to note that the purity is related to the linear entropy, defined by $S_L = 1 - \mathrm{Tr}(\rho_1^2) = 1 - p$. With this relation, the information obtained from the purity is the same that the obtained from the linear entropy, for example, a pure quantum states has $p = 1$ and $S_L = 0$.

One way to evaluate the quantities in Eqs. (A.6), is using the eigenvalues of the reduced density operator, in which case the purity and von Neumann entropy are

$$p = \sum_n \lambda_n^2\,, \quad S_{vN} = -\sum_n \lambda_n\, \log_2(\lambda_n)\,. \tag{A.7}$$

The eigenvalues of the reduced density operator can be obtained numerically using the variational approach. To do this, it is necessary to evaluate the matrix element of each operator in a particular basis, for example, the B-splines functions.

In the one-electron three-dimensional problem, the variational wave function is

$$\Psi^v(\rho, z) = \sum_{i,j} \alpha_{i,j}\, \phi_{i,j}^{3D}(\rho, z)\,, \tag{A.8}$$

Accepted Manuscript

where $\phi^{3D}_{i,j}(\rho, z)$ are the basis functions of the Hilbert space, defined in Eq. (A.5), and $\alpha_{i,j}$ are complex coefficients. For this case we can make a separation of the system in the coordinate, so the reduced matrix operator in the z coordinate is

$$\delta(z, z') = \mathrm{Tr}_\rho(|\Psi^v(\rho, z)\rangle\langle\Psi^v(\rho, z')|) = \int (\Psi^v(\rho, z))^\star \Psi^v(\rho, z')\, \rho\, d\rho\,. \tag{A.9}$$

Replacing Eq. (A.8) in Eq. (A.9) the reduced density operator is

$$\delta(z, z') = \sum_{i,j}\sum_{k,l} \alpha^\star_{i,j}\alpha_{k,l} \int_0^\infty \phi^{3D}_{i,j}(\rho, z)\, \phi^{3D}_{i,j}(\rho, z')\, \rho\, d\rho\,, \tag{A.10}$$

and the matrix elements are given by

$$\begin{aligned}\delta_{n,m} &= \langle n|\delta(z, z')|m\rangle \\ &= \sum_{i,j}\sum_{k,l} \alpha^\star_{i,j}\alpha_{k,l} \int_{-\infty}^\infty \xi_n(z) \left[\left(\int_0^\infty \phi^{3D}_{i,j}(\rho, z)\, \phi^{3D}_{i,j}(\rho, z')\, \rho\, d\rho\right) \xi_m(z')\, dz'\right] dz\,.\end{aligned} \tag{A.11}$$

For this case, we have chosen the B-splines as basis to evaluate the matrix element of the reduced density operator, *i.e.*, $\xi_n(z) = \hat{C}_n B_n(z)$. With this basis the Eq. (A.11) can be re-written in terms of the elements of the superposition matrix of the B-splines. Once the matrix representation of the reduced density operator is made, the eigenvalues can be obtained using numerical algorithms.

For the others cases studied in this work, the procedure to obtain the eigenvalues of the corresponding density operator is analogous, the only difference in each case is how the separation is made. In the case of the one-electron three dimensional problem the separations is made in the coordinate meanwhile in the two-electron one-dimensional case the separation is made in the particle.

Appendix B. Radial Well

It is well known that the exact solution of The Schrödinger equation with the potential in Eq. (13) can be written, for $-V_0 < E < 0$, in term of Bessel functions

$$\psi_{2D}(\rho) = \begin{cases} AJ_0\left(\sqrt{\frac{2m^\star_e}{\hbar^2}(V_0 - |E|)}\,\rho\right) & \text{if} \quad \rho \le a_\rho \\ BK_0\left(\sqrt{\frac{2m^\star_e}{\hbar^2}|E|}\,\rho\right) & \rho > a_\rho \end{cases}. \tag{B.1}$$

Defining $\varepsilon = 2m^\star_e E/\hbar^2$ and $U_0 = 2m^\star_e V_0/\hbar^2$, and using continuity and normalisation conditions we get the transcendental equation for the ground state energy

$$\sqrt{U_0 - |\varepsilon|}\frac{J_1(\sqrt{U_0 - |\varepsilon|}\,a_\rho)}{J_0(\sqrt{U_0 - |\varepsilon|}\,a_\rho)} = \sqrt{|\varepsilon|}\frac{K_1(\sqrt{|\varepsilon|}\,a_\rho)}{K_0(\sqrt{|\varepsilon|}\,a_\rho)}, \tag{B.2}$$

and the normalisation equation

$$1 = \frac{A^2 a_\rho^2}{2} J_1^2(\sqrt{U_0 - |\varepsilon|}\,a_\rho)\left[1 + \frac{U_0 - |\varepsilon|}{|\varepsilon|}\right], \tag{B.3}$$

where J_0, J_1, K_0 and K_1 are the usual Bessel functions [36].

Accepted Manuscript

[1] S. Washburn and R. A. Webb, Advances in Physics **35**, 375 (1986).
[2] N.A.J.M. Kleemans *et al.*, Phys. Rev. Lett. **99**, 146808 (2007).
[3] F. Ding *et al.* , Phys. Rev. B **82**, 075309 (2010).
[4] M. Yamamoto, S. Takada, C. Bäuerle, K. Watanabe, A. D. Wieck and S. Tarucha, Nature Nanotechnology **7**, 247 (2012).
[5] I. Neder, N. Ofek, Y. Chung, M. Heiblum, D. Mahalu, and V. Umansky, Nature **448**, 333 (2007).
[6] R. Ionicioiu, P. Zanardi, F. Rossi, Phys. Rev. A **63**, 050101 (2001).
[7] van der Wiel, W. G. et al. Rev. Mod. Phys. **75**, 122 (2002).
[8] P. Pieri, D. Neilson, and G. C. Strinati, Phys. Rev. B **75**, 113301 (2007).
[9] Vikram V. Deshpande and Marc Bockrath, Nature Physics 4, 314 - 318 (2008).
[10] W. Lei, C. Notthoff, J. Peng, D. Reuter, A. Wieck, G. Bester, and A. Lorke, Phys. Rev. A **105**, 176804 (2010).
[11] R. G. Nazmitdinov, N. S. Simonović, A. R. Plastino and A. V. Chizhov, J. Phys. B: At. Mol. Opt. Phys. **45**, 205503 (2012).
[12] V. V. Ravi Kishore, B. Partoens, and F. M. Peeters. J. Phys.: Condens. Matter **26**, 095501 (2014).
[13] S. Nadj-Perge, V. S. Pribiag, J. W. G. van den Berg, K. Zuo, S. R. Plissard, E. P. A. M. Bakkers, S. M. Frolov, and L. P. Kouwenhoven Phys. Rev. Lett. **108**, 166801 (2012).
[14] J. Avron, I. Herbst, and B. Simon, Phys. Rev. Lett. **39**, 1068 (1977).
[15] J. A. Salas and K. Varga, Phys. Rev. A **89**, 052501 (2014).
[16] Y. K. Ho, Phys. Lett. A **230**, 190 (1997).
[17] Ch. Sikorski and U. Merkt, Phys. Rev. Lett. **62**, 2164 (1989).
[18] M. A. Reed, J. N. Randall, R. J. Aggarwal, R. J. Matyi, T. M. Moore, and A. E. Wetsel, Phys. Rev. Lett. **60**, 535 (1988).
[19] R. Buzcko and F. Bassani, Phys. Rev. B **54**, 2667 (1996).
[20] M. Bylicki and W. Jaskolski, Phys. Rev. B **60**, 15924 (1999).
[21] M. Bylicki, W. Jaskolski, and A. Stachow, Phys. Rev. B **72**, 075434 (2005).
[22] S. Chakraborty and Y. K. Ho, Phys. Rev. A **84**, 032515 (2011).
[23] A. Kuroś and A. Okopińska, Few-Body Syst. **56**, 853-858 (2015).
[24] Y. Sajeev and N. Moiseyev, Phys. Rev. B **78**, 075316 (2008).
[25] M. Genkin and E. Lindroth, Phys. Rev. B **81**, 125315 (2010).
[26] A. Y. Ramos and O. Osenda, J. Phys. B: At. Mol. Opt. Phys. **47**, 015502 (2014).
[27] A. F. Slachmuylders, B. Partoens, W. Magnus, and F. M. Peeters, J. Phys.: Condens. Matter **18**, 3951-3966 (2006).
[28] D. Barettin, A. V. Platonov, A. Pecchia, V. N. Kats, G. E. Cirlin, I. P. Soshnikov, A. D. Bouravleuv, L. Besombes, H. Mariette, M. Auf der Maur, and A. Di Carlo, IEEE J. Sel. Top. Quant. **19**, 1901209 (2013).
[29] S. Bednarek, B. Szafran, T. Chwiej, and J. Adamowski, Phys. Rev. B **68**, 045328 (2003).
[30] H. Bachau, E. Cormier, P. Decleva, J. E. Hansen, and F. Martin. Rep. Prog. Phys. **64** 1815-1942 (2001).
[31] Goldberg Yu.A. and N.M. *Schmidt Handbook Series on Semiconductor Parameters*, vol.2, M. Levinshtein, S. Rumyantsev and M. Shur, ed., (World Scientific, London, 1999) pp. 62-88.
[32] N. Moiseyev, *Non-Hermitian quantum mechanics* (Cambridge University Press, 2011).
[33] P. Zanardi and N. Paunkovic, Phys. Rev. E **74**, 031023 (2006).
[34] K. Życzkowski, P. Horodecki, A. Sanpera, and M. Lewenstein, Phys. Rev. A **58**, 883 (1998).
[35] A. Ramos, PhD Thesis, National University of Córdoba, 2016. Retrieved from *http://www.famaf.unc.edu.ar/wp-content/uploads/2016/09/DFis191.pdf*, published under Creative Commons Agreement.
[36] M. Abramowitz, *Handbook of Mathematical Functions: With Formulas, Graphs, and Mathematical Tables*. (Dover Publications, New York, 1970).
[37] R. Egger and H. Grabert Phys. Rev. B **55**, 9929 (1997).
[38] F. Cavalieri, N. Traverso Ziani, F. Negro and M. Sassetti, J. Phys.: Condens. Matter **26**, 505301

Accepted Manuscript

(2014).
[39] F. M. Pont, A. Bande, L. S. Cederbaum, J. Phys.: Condens. Matter **28**, 075301 (2016).
[40] C. de Boor, *A Practical Guide to Splines*, Springer, New York (1978).

Accepted Manuscript